Toxicology 294 (2012) 27–35

Contents lists available at SciVerse ScienceDirect

Toxicology

journal homepage: www.elsevier.com/locate/toxicol

Susceptibility to gold nanoparticle-induced hepatotoxicity is enhanced in a mouse model of nonalcoholic steatohepatitis

Jung Hwan Hwang[a,1], Soo Jin Kim[c,1], Yong-Hoon Kim[a], Jung-Ran Noh[a], Gil-Tae Gang[a], Bong Hyun Chung[d], Nam Woong Song[c,**], Chul-Ho Lee[a,b,*]

[a] Laboratory Animal Center, Korea Research Institute of Bioscience and Biotechnology (KRIBB), Gwahak-ro 125, Yuseong-gu, Daejeon 305-806, Republic of Korea
[b] University of Science and Technology (UST), Gwahak-ro 125, Yuseong-gu, Daejeon 305-806, Republic of Korea
[c] Center for Nano-Bio Convergence, Korea Research Institute of Standards and Science, Gajeong-ro 209, Yuseong-gu, Daejeon 305-340, Republic of Korea
[d] BioNanotechnology Research Center, Korea Research Institute of Bioscience and Biotechnology and Nanobiotechnology Major School of Engineering, University of Science and Technology, Gwahak-ro 125, Yuseong-gu, Daejeon 305-806, Republic of Korea

ARTICLE INFO

Article history:
Received 1 December 2011
Received in revised form 2 January 2012
Accepted 20 January 2012
Available online 28 January 2012

Keywords:
Gold nanoparticles
Hepatotoxicity
Methionine-choline deficient
Nonalcoholic steatohepatitis

ABSTRACT

Although the safety of gold nanoparticle (AuNP) use is of growing concern, most toxicity studies of AuNPs had focused on their chemical characteristics, including their physical dimensions, surface chemistry, and shape. The present study examined the susceptibility of rodents with healthy or damaged livers to AuNP-induced hepatotoxicity. To induce a model of liver injury, mice were fed a methionine- and choline-deficient (MCD) diet for 4 weeks. Sizes and biodistribution of 15-nm PEGylated AuNPs were analyzed by transmission electron microscopy. Levels of alanine aminotransferase (ALT) and aspartate aminotransferase (AST) were estimated with an automatic chemical analyzer, and liver sections were subjected to pathological examination. Activities of antioxidant enzymes were determined by biochemical assay. Lateral tail vein injection of MCD diet-fed mice with 5 mg kg^{-1} AuNPs significantly elevated the serum ALT and AST levels compared to MCD diet-fed mice injected with mPEG (methylpolyethylene glycol). Similarly, severe hepatic cell damage, acute inflammation, and increased apoptosis and reactive oxygen species (ROS) production were observed in the livers of AuNP-injected mice on the MCD diet; these liver injuries were attenuated in mice fed a normal chow diet. The results suggest that AuNPs display toxicity in a stressed liver environment by stimulating the inflammatory response and accelerating stress-induced apoptosis. These conclusions may point to the importance of considering health conditions, including liver damage, in medical applications of AuNPs.

1. Introduction

The liver is the main target for the toxicity of several compounds, including many medicaments. Drug-induced liver injury is the most frequently cited cause for withdrawal of an approved drug from the market (Lasser et al., 2002) and accounts for up to 25% of liver failure cases (Hoofnagle et al., 1995). Drug-induced liver injury may occur as an unexpected idiosyncratic reaction to a normally non-toxic drug, or may be the direct result of overdosage. Excepting a few cases of intrinsic hepatotoxicity, most cases of drug-induced liver injury are due to idiosyncratic damages caused by the innate and adaptive immune systems (Lee, 2003). Activation of Kupffer cells elicits the release of inflammatory mediators and reactive oxygen species and modulates hepatocyte injury (Laskin et al., 1995; Roberts et al., 2007). In addition, inhibition of macrophage activation or administration of tumor necrosis factor alpha (TNF-α) antagonists protects hepatocytes against paracetamol toxicity, and depletion of Kupffer cells attenuates thioacetamide hepatotoxicity (Laskin et al., 1995; Roberts et al., 2007).

Recently, AuNPs have been the focus of research and practical attention for biomedical applications (Giljohann et al., 2010). They are being administered increasingly to animals and humans parenterally. AuNPs can serve as carriers for the delivery of drugs (Ghosh et al., 2008; Paciotti et al., 2004), genetic materials

Abbreviations: AuNPs, gold nanoparticles; MCD, methionine and choline-deficient; ALT, alanine aminotransferase; AST, aspartate aminotransferase; mPEG, methylpolyethylene glycol; ROS, reactive oxygen species; NC, normal chow; NASH, nonalcoholic steatohepatitis; TG, triglyceride; FASN, fatty acid synthase; SCD1, stearoyl-coenzyme A desaturase 1; TNF-α, tumor necrosis factor alpha; MCP-1, monocyte chemotactic protein-1; SOD, superoxide dismutase; Gpx, glutathione peroxidase.

* Corresponding author at: Laboratory Animal Center, Korea Research Institute of Bioscience and Biotechnology (KRIBB), Gwahak-ro 125, Yuseong-gu, Daejeon 305-806, Republic of Korea. Tel.: +82 42 860 4637; fax: +82 42 860 4609.
** Corresponding author.
E-mail addresses: nwsong@kriss.re.kr (N.W. Song), chullee@kribb.re.kr (C.-H. Lee).
[1] These authors contributed equally to this work.

0300-483X/$ – see front matter © 2012 Elsevier Ireland Ltd. All rights reserved.
doi:10.1016/j.tox.2012.01.013

(Donnelly et al., 2005; Pissuwan et al., 2009), and antigens (Dykman et al., 2004). They are also used as a medicinal or diagnostic agent per se for the treatment of tumors (Bhattacharya and Mukherjee, 2008) or rheumatoid arthritis (Lee et al., 2008; Li et al., 2008). Although there have been controversial results regarding their use, AuNPs are associated with a higher bioavailability, much less acute toxicity, and better scavenging effects than other inorganic nanoparticles.

Nonalcoholic steatohepatitis (NASH) is a chronic progressive liver disease that includes steatosis, balloon degeneration, inflammation, and fibrosis in varying degrees (Farrell and Larter, 2006). NASH is seen in patients with metabolic syndrome, obesity, hyperlipidemia, and type 2 diabetes mellitus (Ludwig et al., 1980). In this study, a rodent model of NASH was elicited by maintaining C57BL/6J mice on a methionine- and choline-deficient (MCD) diet. The MCD diet is a common nutritional method for producing NASH (Rinella and Green, 2004). PEG-coated 15-nm AuNPs were administrated intravenously to mice through lateral tail vein injection, which elicits less toxicity than other administration routes (Zhang et al., 2010). The experimental concentration of AuNPs in our studies was determined on the basis of a previous study in which AuNP injection induced mild acute inflammation and apoptosis in the BALB/c mouse liver (Cho et al., 2009).

2. Materials and methods

2.1. Synthesis and characterization of PEGylated AuNPs

A concentrated (730 mg mL^{-1}) PEGylated AuNP suspension was prepared according to the following procedure. A 250-mL aliquot of a 0.01% (m/v) solution of $HAuCl_4$ (Aldrich, ≥99.9%, Cat. No. C520918) was heated with vigorous stirring in a 500-mL round-bottom flask until the solution temperature reached boiling. After boiling for 15 min, 8.75 mL of 34 mM sodium citrate tribasic dehydrate (Sigma, Cat. No. C8532) was added to the vortex of the solution. The color of the solution changed from pale yellow to burgundy within 10 min. The solution was further boiled for 10 min. Additional stirring was performed for 15 min without heating, to obtain a citrate-stabilized AuNP suspension.

To modify the surface ligand from citrate to mPEG-SH, the AuNP suspension was mixed with an aqueous solution of 0.5 mg mL^{-1} mPEG-SH (Aldrich), at a volume ratio of 1:1. The mixture was stirred for 6 h at room temperature. PEGylated AuNPs were purified from the unbound citrate and mPEG-SH molecules by centrifugation at 13 000 rpm for 30 min. The supernatant was removed and resuspended in Dulbecco's phosphate buffered saline (DPBS) for two treatments. A high concentration of AuNP suspension was prepared by adding a reduced volume of DPBS at the second resuspension step. Deionized (DI) water was used as the resuspension solvent in the preparation of the AuNP suspension for FTIR measurement.

Sizes of individual PEGylated AuNPs were measured with transmission electron microscopy (TEM) and analyzed with ImageJ software (Rasband, 1997–2008). The AuNP size followed a log-normal distribution. An estimated 95% of AuNPs showed diameters within 15.5 ± 1.3 nm, with a 95% confidence interval (Fig. 1A). Broad absorption bands at 1593, 1406, and 1119 cm^{-1}, corresponding to $-CO_2^-$ asymmetric stretching, symmetric stretching, and $-CH_2$ wagging modes in citrate (Max and Chapados, 2004), respectively, disappeared, and a relatively narrow band corresponding to the C–O stretching mode in mPEG-SH (Coates, 2000; Rozenberg et al., 1998) appeared at 1109 cm^{-1} along with other new absorption bands. These findings reflect the complete exchange of surface ligand from citrate to mPEG-SH (Fig. 1B). Additional descriptions of characterization of PEGylated AuNPs can be found in the Supporting Information.

2.2. Animal care and experimental groups

All mice (male, 12-week-old, $n = 37$) were housed individually and maintained at a constant temperature (20–22 °C), with a 12:12-h light: dark schedule. Mice were divided as follows: mice with normal diet (ND) were injected with mPEG at 24 h or 7 days before sacrifice, mice with ND were injected with AuNPs (5 mg kg^{-1}) at 24 h or 7 days before sacrifice, mice with MCD diet for 4 weeks were injected with mPEG at 24 h or 7 days before sacrifice, and mice with MCD diet for 4 weeks were injected with AuNPs (5 mg kg^{-1}) at 24 h or 7 days before sacrifice. The same aged ND groups were used as control for MCD groups. All injections of AuNPs or mPEG were performed intravenously via the lateral tail vein.

Livers were fixed in 10% formalin for histological analysis or quickly frozen in liquid nitrogen, followed by storage in a −80 °C freezer for further experiments. All animal experiments were approved and conducted in accordance with the guidelines of the Institutional Animal Care and Use Committee of the Korea Research Institute of Bioscience and Biotechnology (KRIBB, Daejeon, Korea).

2.3. TEM analysis

Livers were stained *en bloc* with uranyl acetate and embedded in epoxy resin. Ultrathin (60-nm) sections were cut, stained with uranyl acetate and lead citrate, and analyzed with a TEM (JEM-1200EX II, Jeol).

2.4. Quantitative RT-PCR (qRT-PCR) analysis

Total RNA was isolated from mouse liver tissues with Trizol reagent (Invitrogen, Carlsbad, CA). The cDNA was prepared from 1 μg of total RNA with an iScriptTM cDNA synthesis kit (Bio-Rad, Hercules, CA, USA). Each cDNA sample was diluted 5-fold, and a 4-μL aliquot was used in a 10-μL PCR reaction with SYBR Green PCR Master Mix (Takara Bio. Inc., Shiga, Japan) containing primers at concentrations of 10 pM, according to the manufacturer's protocol. PCR reactions were run in duplicate and quantified with an Exicycler 96 (Bioneer, Daejeon, Korea).

Primer sequences for the genes were as follows: for FASN, forward 5′-GAT CCT GGA ACG AGA ACA CGA T-3′, reverse 5′-GAG ACG TGT CAC TCC TGG ACT TG-3′; for SCD1, forward 5′-GCC TCT GGA GCC ACA GAA CT-3′, reverse 5′-GCC CAT TCG TAC ACG TCA TTC-3′; for TNFα, forward 5′-TGG CCT CCC TCT CAT CAG TT-3′, reverse 5′-CCT CCA CTT GGT GGT TTG CT-3′; for MCP1, forward 5′-CTC AGC CAG ATG CAA TCA A-3′, reverse 5′-CTT GGC CAC AAT GGT CTT GA-3′. The cycling conditions were 95 °C for 10 min, followed by 50 cycles of 95 °C for 10 s, and 55–60 °C for 1 min. All expression data were normalized to 18S, and the results were expressed as the fold differences between experimental and control mice.

2.5. Histological analysis

Oil Red O staining was performed on freshly frozen liver sections (8-μm thick) that were rehydrated in PBS and stained with 0.5% Oil Red O (ORO, Sigma Chemical Co., St Louis, MO) for 30 min. Samples were rinsed with PBS and counterstained with hematoxylin for 1 min. Paraffin sections were used for hematoxylin and eosin (H&E) staining. Following deparaffinization and rehydration, sections were stained with hematoxylin for 10 min and eosin for 1 min, according to the manufacturer's protocol.

Immunostaining of Kupffer cells was performed with an anti-F4/80 antibody after antigen retrieval in paraffin-embedded liver sections. Horseradish peroxidase (HRP)-conjugated IgG was used as the secondary antibody (Vectastain Elite ABC kit, Vector Laboratories, Burlingame, CA, USA). Positive macrophages were visualized by DAB (Vector Laboratories). Histopathological diagnosis was performed according to the Standardized system of Nomenclature and Diagnostic Criteria (SSNDC).

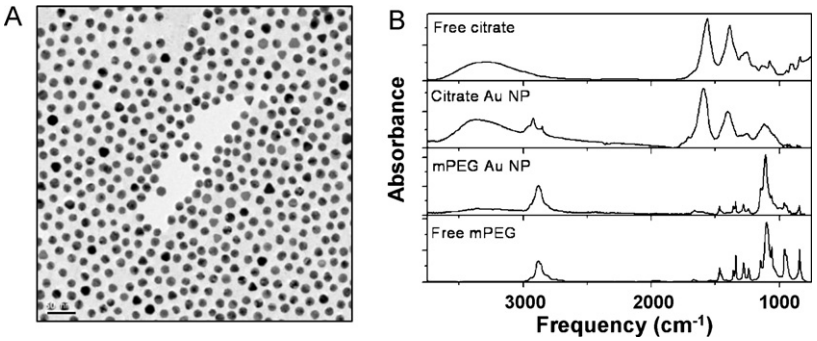

Fig. 1. TEM image and FT-IR absorption. (A) The size of the PEGylated 15-nm AuNPs was determined by TEM. Scale bar is 50 μm. (B) FT-IR absorption spectra of dried films prepared from free ligand solutions and AuNP suspension.

2.6. Apoptosis analysis

Paraffin-embedded liver sections (5-μm thickness) were deparaffinized in xylene and hydrated in graded ethanol. Liver sections were stained with terminal deoxynucleotideyl transferase-mediated dUTP nick end-labeling (TUNEL) kits, according to the manufacturer's procedure (Millipore, MA, USA). Ten random fields from three slides per group were examined for TUNEL-positive cell counts. Caspase-3 staining was performed on tissue sections that were incubated overnight at 4 °C with a specific primary antibody (1:100) against cleaved caspase-3 (Cell Signaling Technology, Inc., Danvers, MA, USA). Stained liver sections were visualized with a Vectastain Elite ABC kit (Vector Laboratories) and DAB (Vector Laboratories) and briefly counterstained with hematoxylin before mounting.

2.7. Plasma analysis

At the end of the experimental period, mice were sacrificed by cervical dislocation. Blood samples were taken from the orbital venous congestion to determine concentrations of the plasma biomarkers. Plasma was prepared by centrifugation of the blood at 10 000 × *g* for 5 min at 4 °C. Plasma was stored at −70 °C prior to analysis. Plasma AST and ALT levels were measured with an automatic chemical analyzer (Hitachi 7150, Japan).

2.8. Enzyme assay

Liver tissue was homogenized in sucrose buffer (0.25 mol L^{-1}). Homogenates were centrifuged at 600 × *g* for 10 min to remove the nuclear fraction. The remaining separated supernatant was recentrifuged at 10 000 × *g* for 20 min, to collect the mitochondrial pellet for catalase (CAT) assay. The supernatant was further ultracentrifuged at 100 000 × *g* for 1 h to obtain the cytosolic supernatant for use in superoxide dismutase (SOD) and glutathione peroxidase (GPx) assays. Protein concentrations in the supernatant and liver fractions were determined by the Bradford method using bovine serum albumin as the standard.

The CAT activity was measured by Aebi's method (Aebi, 1974) with a slight modification, whereby hydrogen peroxide decomposition to yield water and oxygen was measured. The CAT activity was expressed as the change (decrease) in H_2O_2 concentration (in μM) per milligram of protein per minute. GPx activity was assayed with the Paglia and Valentine method (Paglia and Valentine, 1967) with a slight modification, and was expressed as the concentration (in nM) of oxidized NADPH per milligram of protein per minute.

The SOD activity was measured by a modified version of the method developed by Marklund and Marklund (1974), which measures a color change induced by the auto-oxidation of pyrogallol. One unit was determined as the amount of enzyme that inhibited the oxidation of pyrogallol by 50%. The activity was expressed as units per milligram of protein.

2.9. ROS measurement

Total levels of ROS production were determined by the oxidative conversion of nonfluorescent 2′,7′-dichlorofluorescein diacetate (H_2DCFDA) to highly fluorescent 2′,7′-dichlorofluorescein (DCF). Liver extracts (100 μL) were incubated at 37 °C for 60 min with 100 μL of 2 mM H_2DCFDA (Invitrogen) in PBS. Fluorescence was recorded at 485 nm (excitation) and 527 nm (emission) with a Victor3 1420 Multilabel Counter (Perkin Elmer, MA, USA) and normalized to protein content. Hydrogen peroxide was measured with a hydrogen peroxide assay kit (BioVision, CA, USA), according to the manufacturer's instructions. Briefly, liver tissues were lysed in sucrose buffer (0.25 mol L^{-1}). The resulting extract was mixed with a 50-μL reaction mixture containing assay buffer, OxiRed probe solution, and HRP solution, and incubated at room temperature for 10 min. Concentrations of H_2O_2 were determined with a microplate reader at 570 nm.

2.10. Lipid peroxidation

Levels of hepatic lipid peroxide were determined by immunofluorescence staining with an antibody against 4-hydroxy-2-nonenal (4-HNE) (Abcam, Cambridge, UK). Liver sections were incubated with primary antibody and visualized with Alexa Fluoro 546-nm antibody (Invitrogen, CA, USA). Stained sections were analyzed by confocal microscopy (400×) (LSM510 META; Carl Zeiss, Jena, Germany). All measurements were performed by blinded observers.

2.11. Western blot analysis

Liver tissues were homogenized in sucrose buffer (0.25 mol L^{-1}). Homogenates were centrifuged at 600 × *g* for 10 min to remove the nuclear fraction. The remaining separated supernatant was recentrifuged at 10 000 × *g* for 20 min to collect the mitochondrial pellet. The supernatant was ultracentrifuged at 100 000 × *g* for 1 h to obtain the cytosolic supernatant. Proteins from the mitochondria and cytosolic fractions were separated by 10–12% SDS-polyacrylamide gel electrophoresis, and transferred to PVDF membranes. Anti-cytochrome c (Cell Signaling Technology), anti-complex II (SDHA; Invitrogen, CA, USA), and anti-α-tubulin (Cell Signaling Technology) antibodies were used for the immunoblotting assay as primary antibodies.

2.12. Statistical analysis

Numerical data are presented as mean values ± SEM. Comparisons between groups were performed with a two-tailed Student's *t*-test or one-way ANOVA. The threshold of significance was set at $P < 0.05$.

3. Results

3.1. Distribution of AuNPs in the mouse liver

Using TEM analysis, we determined the localization of AuNPs in the livers of mice at 24 h and 7 d after injection. Clusters of AuNPs were detected in Kupffer cells, but not in hepatocytes, at 24 h postinjection (Fig. 2A–C). AuNPs were more clustered at 7 d postinjection compared with those observed at 24 h postinjection (Fig. 2D and E). Highly magnified TEM images provided further information about the cellular localization of AuNPs. Most AuNPs were observed in vesicles or lysosomes of Kupffer cells at 24 h postinjection, and they remained visible through 7 d postinjection (Fig. 2C and F).

3.2. Effect of AuNPs on MCD diet-mediated fat accumulation

Mice that were fed an MCD diet for 4 weeks exhibited an increase in lipid accumulation (Fig. 3 and Fig. S4). AuNPs (5 mg kg^{-1}) were administrated intravenously via the tail vein, and mice were sacrificed at 24 h or 7 d postinjection to investigate the effects of AuNPs on triglyceride (TG) accumulation. Histological results obtained with Oil Red O showed that injection with AuNP had no effect on TG accumulation in the livers of NC- or MCD diet-fed mice at either time point (Fig. 3A and Fig. S4). This result was further supported by the unchanged expression of genes related to lipogenesis, including fatty acid synthase (FASN) and stearoyl-coenzyme A desaturase 1 (SCD1) (Flowers and Ntambi, 2008; Loftus et al., 2000) (Fig. 3B and C).

3.3. Increased hepatotoxicity of AuNPs in mice fed the MCD diet for 4 weeks

Serum ALT and AST levels are common markers for hepatic toxicity: levels of these proteins are rapidly increased in sera when the liver is damaged by any cause, including hepatitis or hepatic cirrhosis (Sheth et al., 1998). The ALT and AST levels of the mPEG control groups fed the MCD diet were increased approximately 4- and 3-fold, respectively, compared with mice fed the NC diet. Interestingly, in the NC condition, AuNP-treated mice showed slightly lower levels of these two enzymes than mPEG-treated mice (Fig. 4A and B). However, the MCD diet-induced ALT and AST increases were significantly enhanced in AuNP-injected groups compared with the mPEG-injected groups (Fig. 4A and B). These results suggest that the hepatotoxicity of AuNPs is much higher in the MCD diet-fed mice than in NC-fed mice.

3.4. Increased inflammatory response in livers from AuNP-treated mice fed the MCD diet for 4 weeks

To investigate the underlying mechanism of the increased toxicity of AuNPs in MCD diet-fed mice, liver sections from all groups were stained with H&E. Histopathological examination showed no evidence of inflammation in the livers of mPEG- or AuNP-injected mice fed the NC diet (Fig. 5A). Mild mixed inflammation was observed in the livers of mPEG-injected mice fed the MCD diet for 4 weeks. However, the livers of MCD diet-fed mice injected with AuNPs showed severe mixed lobular inflammation with a definite acute component after 24 h and 7 d (Fig. 5 and Fig. S5A). The enhanced inflammatory signs in mice fed the MCD diet at 24 h after AuNP injection were further supported by liver sections stained

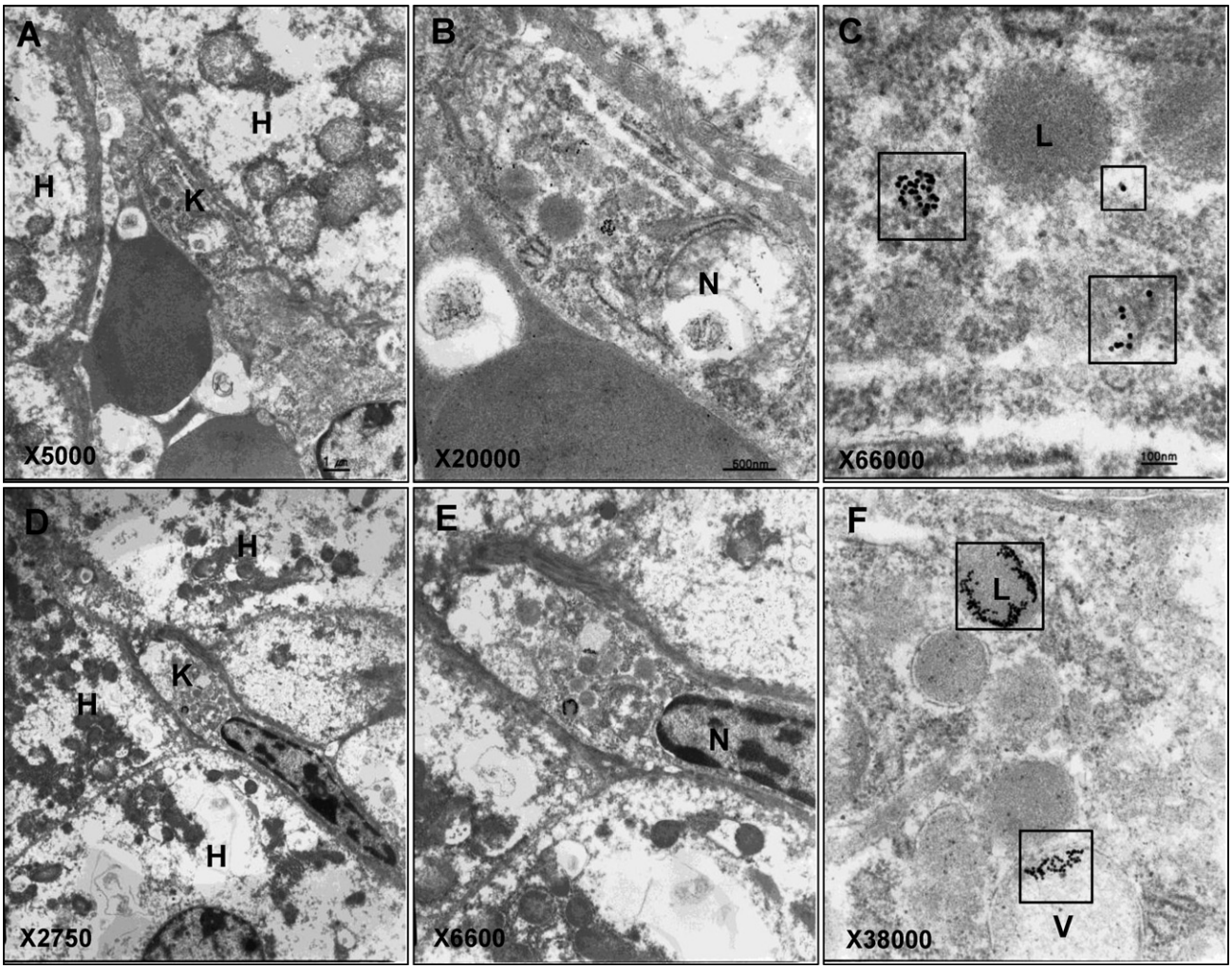

Fig. 2. TEM images of liver tissues at 24 h or 7 d after intravenous injection with PEGylated AuNPs. The micrographs show PEGylated AuNPs trapped by Kupffer cells and their subcellular localization. Magnifications of liver tissues at 24 h after AuNPs injection are 5000× (A), 20 000× (B), and 66 000× (C). Magnifications at 7 d are 2750× (D), 6600× (E), and 3800× (F). H, hepatocyte; K, Kupffer cell; N, nucleus; L, lysosome; and V, vesicle.

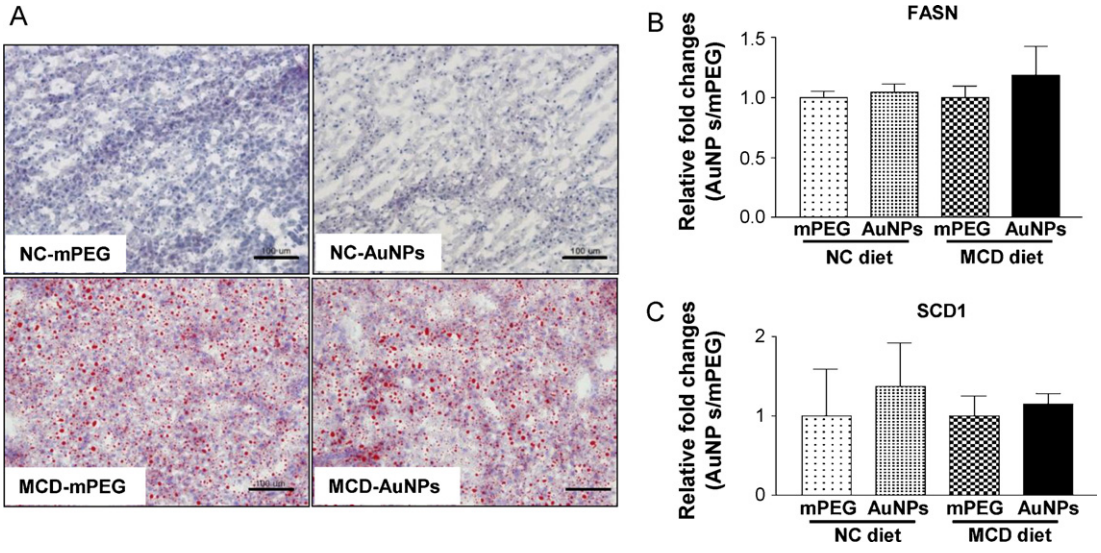

Fig. 3. TG accumulation in the livers of mPEG- and AuNP-injected mice. (A) Representative liver sections from mice injected with mPEG or AuNP after 24 h with/without MCD diet, stained with Oil Red O. Red colors indicate accumulated TG. Scale bar is 100 μm. Estimated gene expression of FASN (B) and SCD1 (C) in liver from mice injected with mPEG ($n = 7$) or 5 mg kg^{-1} AuNPs ($n = 7$), by qRT-PCR with specific primers. Data are expressed as fold changes (AuNPs/mPEG).

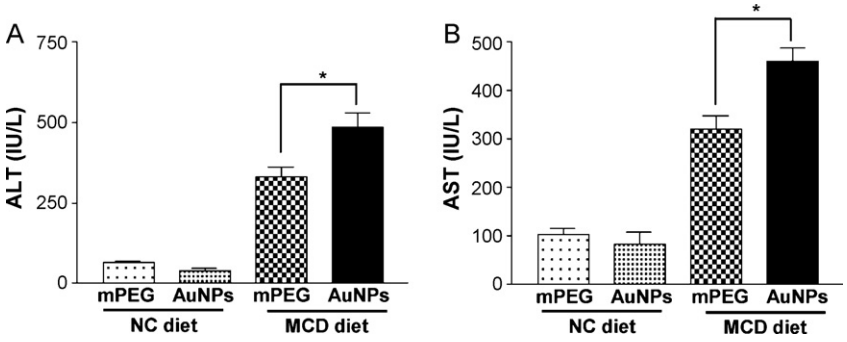

Fig. 4. Elevated ALT and AST levels after AuNP injection in MCD diet-fed mice. (A and B) Plasma ALT (A) and AST (B) levels of mPEG or AuNP groups fed with the NC diet (mPEG, $n = 3$; AuNPs, $n = 3$) or the MCD diet (mPEG, $n = 7$; AuNPs, $n = 7$), determined with an automatic chemical analyzer at 24 h after injection, respectively. Mice used in all experiments were male. $^{*}P < 0.05$.

with F4/80 antibody, which specifically stains Kupffer cells (Fig. 5B) (Nikfarjam et al., 2005). Consistent results were observed in the livers of mice at 7 d after AuNP injection (Fig. S5B).

The mRNA levels of TNF-α and monocyte chemotactic protein-1 (MCP-1) were investigated by qRT-PCR. Four weeks of the MCD diet treatment resulted in increased hepatic TNF-α mRNA levels compared with the NC diet treatment (Fig. 5C and D). The MCD diet-induced upregulation of TNF-α and MCP-1 mRNAs was further elevated in the livers of mice at 24 h after AuNP injection (Fig. 5C and D). These findings suggest that injection with AuNPs produces an increased inflammatory response only in mice with damaged livers.

3.5. Increased apoptosis in livers from AuNP-injected mice fed the MCD diet for 4 weeks

Cytokine overexpression contributes to hepatocellular apoptosis during NASH (Leist et al., 1998). The effects of AuNPs on apoptosis were determined with TUNEL analysis, by counting the number of positively stained cells in 10 randomly selected high-power (200×) fields per slide of liver samples from five mice. Low numbers of TUNEL-positive cells were detected in both mPEG- and AuNP-injected groups fed the NC diet, but the mPEG-injected, MCD-fed group showed increased TUNEL-positive staining (Fig. 6A). AuNP injection very strongly enhanced the MCD diet-induced

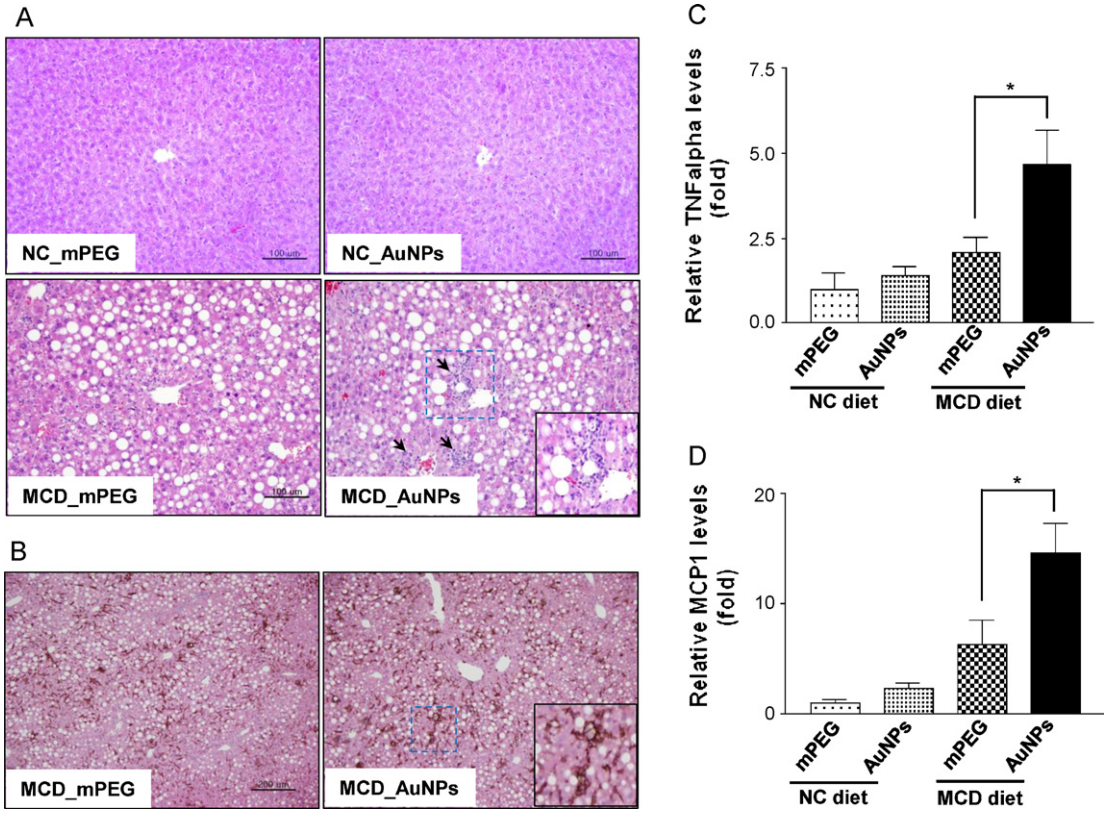

Fig. 5. Increased inflammatory cells in livers of mice injected with AuNPs for 1 day. (A) Representative liver sections from mice injected with mPEG or AuNPs (5 mg kg^{-1}) for 24 h in the NC- or MCD-diet condition, stained with hematoxylin and eosin (H&E). (A) Inflammatory foci were highly visible in AuNP-injected groups fed the MCD diet. The blue dotted square is enlarged and indicates inflammatory foci. (B) Liver sections from mice injected with mPEG or AuNPs for 24 h in the MCD-diet condition, stained with anti-F4/80 to detect Kupffer cells. (C and D) Estimated gene expression of TNF-α (B) and MCP1 (C) in the livers of mice injected with mPEG or AuNP with the NC diet (mPEG, $n = 3$; AuNPs, $n = 3$) or the MCD diet (mPEG, $n = 7$; AuNPs, $n = 7$), by qRT-PCR with specific primers. Data are expressed as fold changes (AuNPs/mPEG). $^{*}P < 0.05$. (For interpretation of the references to color in this figure legend, the reader is referred to the web version of the article.)

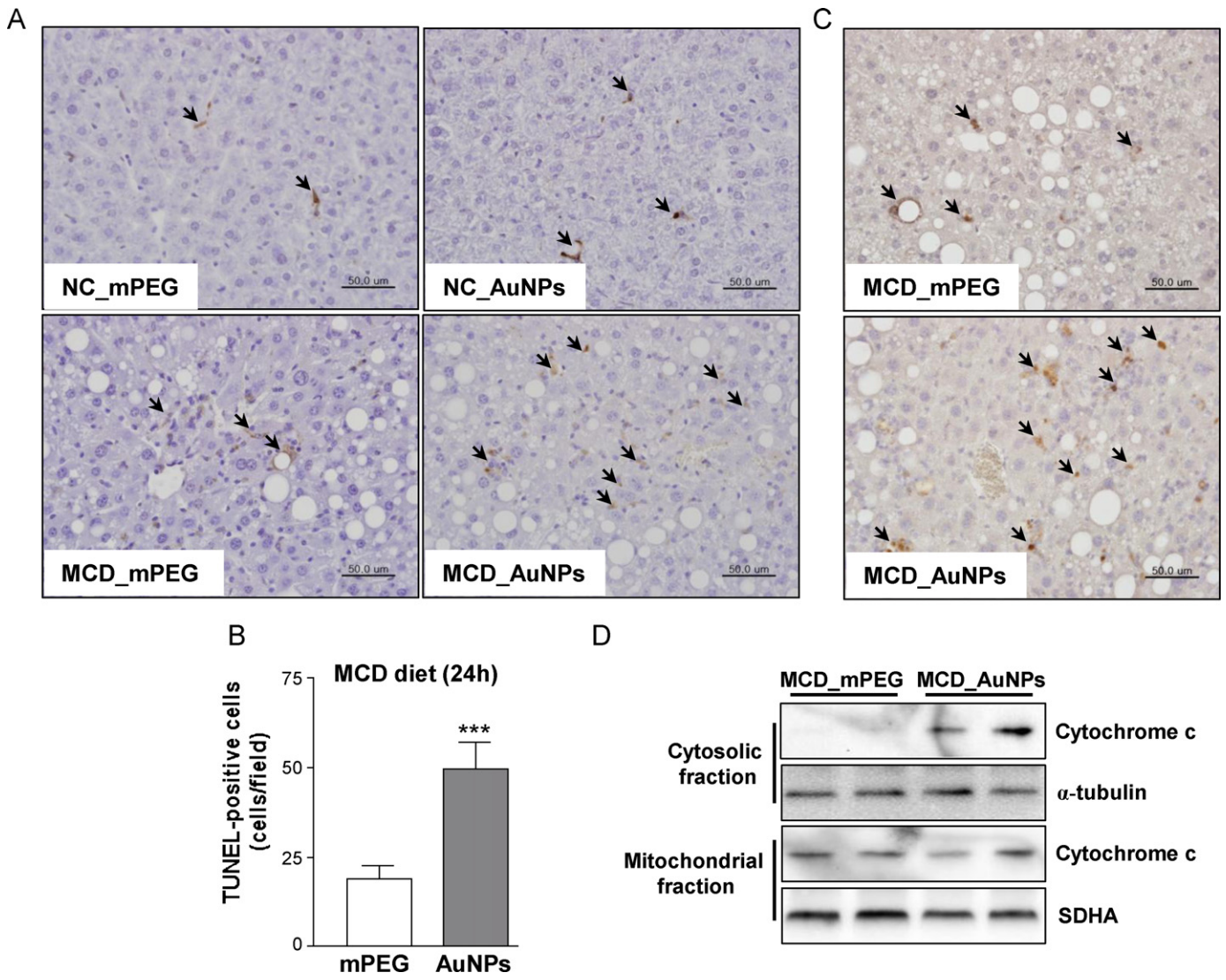

Fig. 6. Accelerated apoptosis after AuNP injection under the MCD-diet condition. (A) TUNEL assay of liver sections from mice injected with mPEG or AuNPs (5 mg kg^{-1}) for 24 h with the NC or MCD diet. Arrow indicates TUNEL-positive cells. (B) TUNEL-positive cells were counted in 10 randomly selected high-power (200×) fields per liver sample slide from five mice. ***$P < 0.001$. (C) Liver sections at 24 h after injection with mPEG or AuNPs in the MCD-diet condition, stained with a specific antibody against cleaved caspase-3. Arrow indicates apoptotic cells. Scale bars are 50 μm. (D) Release of cytochrome c from mitochondria into cytoplasm was estimated in cytosolic and mitochondrial liver fractions of the indicated groups by immunoblotting with a specific antibody against cytochrome c.

apoptosis at 24 h (Fig. 6A) and 7 d (Fig. S6A), as indicated by increased TUNEL staining. With the MCD diet, the mean numbers of TUNEL-positive cells in each field per slide for the mPEG and AuNPs groups were 18.9 ± 14.4 and 49.8 ± 23.2, respectively (Fig. 6B).

Previous studies suggest that TNF-α induces apoptotic cell death via activation of procaspase-8, which stimulates the activation of caspase-3 protein (Wang et al., 2008). Thus, liver sections from all groups were stained with an antibody against cleaved caspase-3, which is the active form of this protein. Results were consistent with the TUNEL study: active caspase-3 levels were dramatically elevated in the livers of the AuNP-injected groups compared with the mPEG-injected groups at 24 h and 7 d postinjection under the MCD diet condition (Fig. 6 and Fig. S6B).

Cytochrome c levels in the mitochondrial and cytosolic fractions of livers were tested in all groups with an immunoblot assay. Release of upregulated cytochrome c from mitochondria into the cytoplasm was only observed in the livers of AuNP-injected mice fed with the MCD diet (Fig. 6D). These data show that the AuNP-mediated increase of apoptosis in MCD-diet mice is due to intrinsic and extrinsic pathways, with one being dependent and the other independent of mitochondrial function.

3.6. Increased ROS production in livers from AuNP-treated mice fed the MCD diet for 4 weeks

In addition to producing cytokines, activated Kupffer cells are the major source of ROS in the liver (Bilzer et al., 1999). Thus, it could be predicted that liver ROS levels would be increased in AuNP-injected mice fed the MCD diet. Total ROS productions in the liver extracts of the four groups were estimated by detecting the oxidation-induced fluorescence emitted by the dye H_2DCFDA. No difference was observed in the livers of mice fed with the NC or MCD diet after mPEG injection, indicating that endogenous ROS generation was not affected by feeding with the MCD diet for 4 weeks (Fig. 7A). However, AuNP injection led to significantly higher total ROS levels in the damaged liver condition (Fig. 7A).

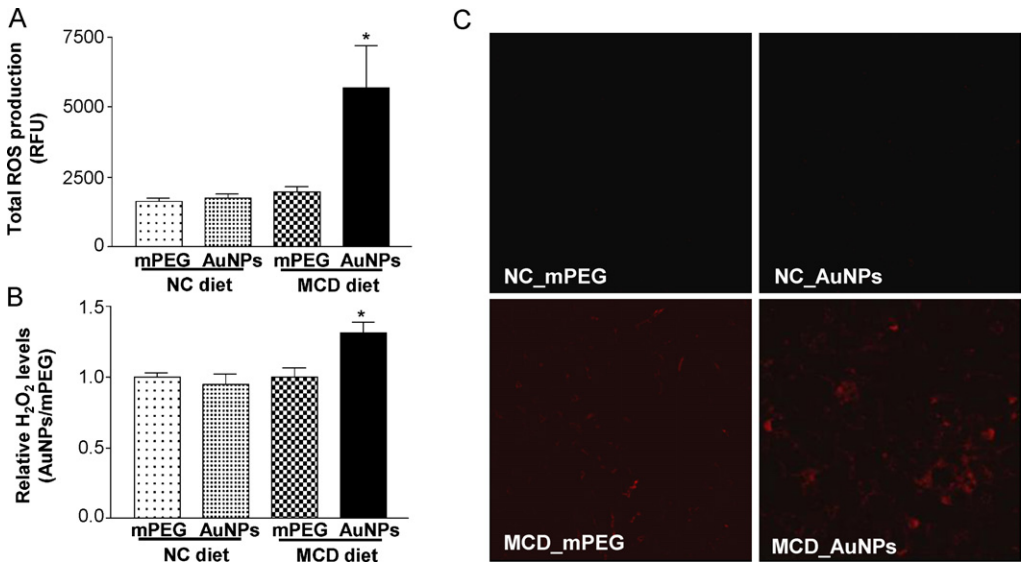

Fig. 7. Increased ROS production after injection with AuNPs under the MCD-diet condition. (A) Total ROS production was measured as the oxidative conversion of H_2DCFDA to highly fluorescent 2′,7′-dichlorofluorescein (DCF), as described in the Supporting Information. (B) H_2O_2 levels were determined with a hydrogen peroxide assay kit. (C) Levels of hepatic lipid peroxide were determined by immunofluorescence staining using antibody against 4-hydroxy-2-nonenal (4-HNE).

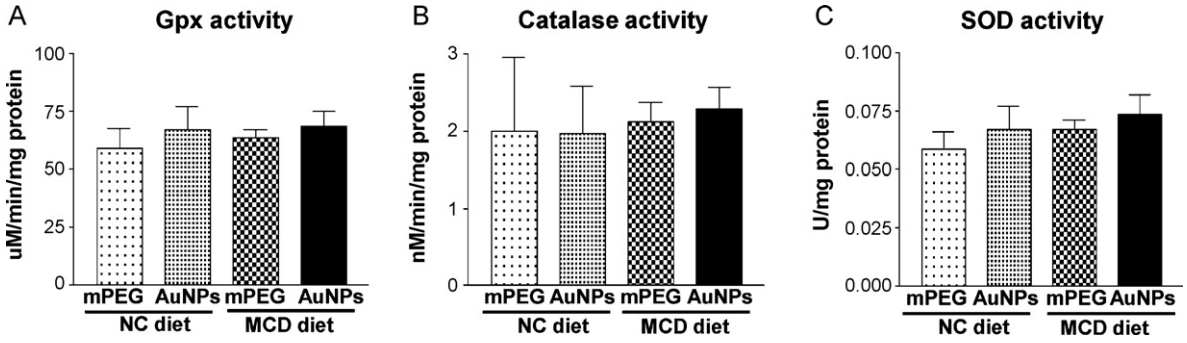

Fig. 8. No significant differences in antioxidant enzyme expression occur among groups injected with mPEG ($n = 5$) or AuNP ($n = 5$) at 24 h postinjection, under the NC- or MCD-diet condition. (A) Glutathione peroxidase (Gpx) activity, (B) catalase (CAT) activity, and (C) superoxide dismutase (SOD) activity were measured in liver lysates from each group.

The concentrations of H_2O_2 and the fluorescence intensity of lipid peroxidation, which indicate total ROS generation, were also higher in AuNP-injected groups fed with the MCD diet compared with the other groups (Fig. 7B and C).

Under normal health conditions, cells can defend themselves against ROS increases using antioxidant enzymes, such as superoxide dismutase (SOD) (Mittler, 2002), catalase (Dorval and Hontela, 2003), and glutathione peroxidase (Gpx) (Gouaze et al., 2002), Therefore, the activities of these three enzymes were tested in liver extract isolates from all groups to determine whether injection with AuNPs caused a change in their activity levels. No significant difference was observed among all groups, which indicated that the AuNP-induced ROS increase was not related to the gene expression of antioxidant enzymes (Fig. 8A–C and Fig. S7A–C).

4. Discussion

A whole organism is much more complex than a single cell. Therefore, toxicological studies in various environments are required to assess the safety of nanoparticles at the animal level. In this study, PEGylated AuNPs of approximately 15 nm in size were synthesized as biologically compatible. The susceptibility of mice with damaged livers (i.e., a mouse model of NASH, which is a cause of chronic liver disease) (Sanyal, 2001) to AuNP-mediated hepatotoxicity was investigated. The results showed that susceptibility to AuNP-induced hepatotoxicity can depend on the health condition of the target animal.

The ALT and AST levels in blood are common measures used to estimate hepatotoxicity in the experimental setting. Serum ALT and AST levels increase rapidly when the liver is damaged by any cause, including hepatitis or hepatic cirrhosis (Sheth et al., 1998). Based on these reports, we investigated if AuNPs induced serum ALT and AST levels in normal- and damaged liver environments. In our study, serum ALT and AST levels in NC diet-fed mice remained in the normal range at 24 h or 7 d after AuNP administration, suggesting that AuNPs are nontoxic in the normal diet condition. However, these enzymes were increased in serum from mice fed the MCD diet for 4 weeks. Interestingly, MCD-mediated ALT and AST increases were further elevated (up to approximately two times) after AuNP administration, indicating that AuNP treatment could accelerate the toxicity in rodents with diseased livers.

To verify further the major mechanism leading to hepatotoxicity by AuNPs in the diseased liver condition, we estimated the steatosis grade, lobular inflammation, and apoptotic cell death, which are the major features of NASH, in each group. In the NC condition, no differences in the steatosis grade, lobular inflammation, or apoptosis were observed in mice treated with mPEG or PEGylated AuNPs. These results suggest that AuNP treatment

does not stimulate the inflammatory response or apoptosis in the healthy condition. MCD diets induce hepatic TG accumulation by inhibiting mitochondrial beta-oxidation of fatty acids and blocking hepatic export of very-low-density lipoprotein (Anstee and Goldin, 2006). This inhibited that lipid disposal causes hepatic TG accumulation in lean mice. Interestingly, inhibiting TG synthesis improves hepatic steatosis, but exacerbates liver damage, in obese mice fed an MCD diet (Yamaguchi et al., 2007). This investigation would suggest that TG accumulation may be a protective mechanism to prevent progressive liver damage, but does not exacerbate liver damage. Accumulated TG levels in AuNP-injected mice fed the MCD diet for 4 weeks were not different from levels of the vehicle groups. However, more MCD diet-mediated inflammatory foci and apoptosis-positive cells were found in the livers of AuNP-injected mice than in livers from vehicle-injected mice. These findings suggest that AuNP-induced hepatotoxicity results from increased inflammatory response and apoptosis, but not from accumulated TG contents.

Although further studies are needed to investigate the underlying mechanism of the increased inflammatory response and apoptosis, the elevated ROS production in AuNP-treated groups fed the MCD diet may be a causing factor for the initiation of liver damage. Many studies have shown that ROS can induce apoptosis in various cell systems (Herrera et al., 2001; Simon et al., 2000) and under inflammatory conditions (Simon et al., 2000). TNF-α signaling stimulated by ROS has been suggested as one mechanism for apoptotic induction in the inflammatory response (Simon et al., 2000). The observed upregulation of TNF-α and MCP-1 mRNA levels in MCD diet-fed mice after administration of AuNPs may have been mediated by increased ROS production.

Kupffer cells are included in the first line of defense against debris and microbial products absorbed via the intestines. They cleanse the blood of foreign materials and toxic substances (Wheeler, 2003). Kupffer cells are activated from a resting state when they encounter foreign materials and also stimulated in nutritional model of NASH, leading to upregulation of TNF-α (Su, 2002). TNF-α is thought to regulate Kupffer cell activation through both autocrine and paracrine mechanisms (Kitamura et al., 2002). In addition, recent study suggested that enhancement of signaling following activation of Kupffer cells may be critical in the pathogenesis of hepatic steatosis and fibrosis in MCD-induced NASH model (Tomita et al., 2006). Therefore, in the present study, it is noteworthy that AuNPs treatment in stressed liver led to upregulated TNF-α expression, resulting in activation of Kupffer cells and liver injury. This hypothesis is further evidenced by distribution of injected AuNPs which are mostly detected in Kupffer cells, but not in hepatocytes. Consistent with our result, other study also demonstrated that PEG-coated AuNPs were initially trapped in the liver Kupffer cells by phagocytosis (Cho et al., 2009). Therefore, our study shows that Kupffer cell activation may be a critical element in the AuNP-mediated liver damage after MCD diet.

5. Conclusions

Following intravenous injection, most of the small AuNPs were rapidly trapped by Kupffer cells in the liver. The AuNPs clustered into lysosomes or vesicles of the cells. Under conditions of normal health, the Kupffer cells remained in their resting state after AuNP injection. However, Kupffer cells were stimulated by exposure to AuNPs via undefined mechanisms under the stressed condition. AuNP-induced Kupffer cell activation led to increased recruitment of other monocytes and maturation of these cells, which subsequently upregulated the secretion of various cytokines. The secreted cytokines mediated increased cell death by necrosis and apoptosis, and abnormal ROS production resulted in additional liver damage. Thus, in a stressed liver environment, AuNPs display toxicity by stimulating the inflammatory response and accelerating stress-induced apoptosis, although they do not exert noticeable toxicity to normal livers.

The results suggest that the individual health condition and disease status should be considered when applying AuNPs for therapeutic interventions to avoid unexpected side effects. Further studies of different disease conditions are necessary to understand the safety of nanomaterials in biomedical and clinical applications.

Conflict of interest

The authors declare that there are no conflicts of interest.

Acknowledgments

This study was supported by a grant from KRIBB Research Initiative Program of Korea, and by the Development of Characterization Techniques for Nano-materials Safety Project of KRCF and Nano Material Technology Development Program (Green Nano Technology Development Program) (2011-0020504) (NWS). The authors thank Ji-Sun Moon and Dong-Hee Choi for their technical assistance.

Appendix A. Supplementary data

Supplementary data associated with this article can be found, in the online version, at doi:10.1016/j.tox.2012.01.013.

References

Lasser, K.E., Allen, P.D., Woolhandler, S.J., Himmelstein, D.U., Wolfe, S.M., Bor, D.H., 2002. Timing of new black box warnings and withdrawals for prescription medications. JAMA 287, 2215–2220.
Hoofnagle, J.H., Carithers Jr., R.L., Shapiro, C., Ascher, N., 1995. Fulminant hepatic failure: summary of a workshop. Hepatology 21, 240–252.
Lee, W.M., 2003. Drug-induced hepatotoxicity. N. Engl. J. Med. 349, 474–485.
Laskin, D.L., Gardner, C.R., Price, V.F., Jollow, D.J., 1995. Modulation of macrophage functioning abrogates the acute hepatotoxicity of acetaminophen. Hepatology 21, 1045–1050.
Roberts, R.A., Ganey, P.E., Ju, C., Kamendulis, L.M., Rusyn, I., Klaunig, J.E., 2007. Role of the Kupffer cell in mediating hepatic toxicity and carcinogenesis. Toxicol. Sci. 96, 2–15.
Giljohann, D.A., Seferos, D.S., Daniel, W.L., Massich, M.D., Patel, P.C., Mirkin, C.A., 2010. Gold nanoparticles for biology and medicine. Angew. Chem. Int. Ed. Engl. 49, 3280–3294.
Ghosh, P., Han, G., De, M., Kim, C.K., Rotello, V.M., 2008. Gold nanoparticles in delivery applications. Adv. Drug Deliv. Rev. 60, 1307–1315.
Paciotti, G.F., Myer, L., Weinreich, D., Goia, D., Pavel, N., McLaughlin, R.E., Tamarkin, L., 2004. Colloidal gold: a novel nanoparticle vector for tumor directed drug delivery. Drug Deliv. 11, 169–183.
Donnelly, J.J., Wahren, B., Liu, M.A., 2005. DNA vaccines: progress and challenges. J. Immunol. 175, 633–639.
Pissuwan, D., Niidome, T., Cortie, M.B., 2009. The forthcoming applications of gold nanoparticles in drug and gene delivery systems. J. Control Release 149, 65–71.
Dykman, L.A., Sumaroka, M.V., Staroverov, S.A., Zaitseva, I.S., Bogatyrev, V.A., 2004. Immunogenic properties of the colloidal gold. Izv. Akad. Nauk. Ser. Biol., 86–91.
Bhattacharya, R., Mukherjee, P., 2008. Biological properties of naked metal nanoparticles. Adv. Drug Deliv. Rev. 60, 1289–1306.
Lee, H., Lee, K., Kim, I.K., Park, T.G., 2008. Synthesis, characterization, and in vivo diagnostic applications of hyaluronic acid immobilized gold nanoprobes. Biomaterials 29, 4709–4718.
Li, S., Zhang, R., Li, P., Yi, W., Zhang, Z., Chen, S., Su, S., Zhao, L., Hu, C., 2008. Development of a novel method to measure macrophage migration inhibitory factor (MIF) in sera of patients with rheumatoid arthritis by combined electrochemical immunosensor. Int. Immunopharmacol. 8, 859–865.
Farrell, G.C., Larter, C.Z., 2006. Nonalcoholic fatty liver disease: from steatosis to cirrhosis. Hepatology 43, S99–S112.
Ludwig, J., Viggiano, T.R., McGill, D.B., Oh, B.J., 1980. Nonalcoholic steatohepatitis: Mayo Clinic experiences with a hitherto unnamed disease. Mayo Clin. Proc. 55, 434–438.
Rinella, M.E., Green, R.M., 2004. The methionine-choline deficient dietary model of steatohepatitis does not exhibit insulin resistance. J. Hepatol. 40, 47–51.
Zhang, X.D., Wu, H.Y., Wu, D., Wang, Y.Y., Chang, J.H., Zhai, Z.B., Meng, A.M., Liu, P.X., Zhang, L.A., Fan, F.Y., 2010. Toxicologic effects of gold nanoparticles in vivo by different administration routes. Int. J. Nanomed. 5, 771–781.

Cho, W.S., Cho, M., Jeong, J., Choi, M., Cho, H.Y., Han, B.S., Kim, S.H., Kim, H.O., Lim, Y.T., Chung, B.H., 2009. Acute toxicity and pharmacokinetics of 13 nm-sized PEG-coated gold nanoparticles. Toxicol. Appl. Pharmacol. 236, 16–24.
Rasband, W., 1997–2008. ImageJ. U.S. National Institutes of Health, Bethesda, MD, USA, http://rsb.info.nih.gov/ij/.
Max, J.J., Chapados, C., 2004. Infrared spectroscopy of acetone–water liquid mixtures. II. Molecular model. J. Chem. Phys. 120, 6625–6641.
Coates, J., 2000. Interpretation of infrared spectra, a practical approach. In: Mayers, R.A. (Ed.), Encyclopedia of Analytical Chemistry. , pp. 10815–10837.
Rozenberg, M., Loewenschuss, A., Marcus, Y., 1998. IR spectra and hydration of short-chain polyethyleneglycols. Spectrochim. Acta A 54, 1819–1826.
Aebi, H., 1974. Methods of Enzymatic Analysis. Academic Press, New York, 673–684.
Paglia, D.E., Valentine, W.N., 1967. Studies on the quantitative and qualitative characterization of erythrocyte glutathione peroxidase. J. Lab. Clin. Med. 70, 158–169.
Marklund, S., Marklund, G., 1974. Involvement of superoxide anion radical in the auto oxidation of pyrogallol and a convenient assay for superoxide dismutase. Eur. J. Biochem. 47, 469–474.
Flowers, M.T., Ntambi, J.M., 2008. Role of stearoyl-coenzyme A desaturase in regulating lipid metabolism. Curr. Opin. Lipidol. 19, 248–256.
Loftus, T.M., Jaworsky, D.E., Frehywot, G.L., Townsend, C.A., Ronnett, G.V., Lane, M.D., Kuhajda, F.P., 2000. Reduced food intake and body weight in mice treated with fatty acid synthase inhibitors. Science 288, 2379–2381.
Sheth, S.G., Flamm, S.L., Gordon, F.D., Chopra, S., 1998. AST/ALT ratio predicts cirrhosis in patients with chronic hepatitis C virus infection. Am. J. Gastroenterol. 93, 44–48.
Nikfarjam, M., Muralidharan, V., Su, K., Malcontenti-Wilson, C., Christophi, C., 2005. Patterns of heat shock protein (HSP70) expression and Kupffer cell activity following thermal ablation of liver and colorectal liver metastases. Int. J. Hyperthermia 21, 319–332.
Leist, M., Gantner, F., Kunstle, G., Wendel, A., 1998. Cytokine-mediated hepatic apoptosis. Rev. Physiol. Biochem. Pharmacol. 133, 109–155.
Wang, L., Du, F., Wang, X., 2008. TNF-alpha induces two distinct caspase-8 activation pathways. Cell 133, 693–703.
Bilzer, M., Jaeschke, H., Vollmar, A.M., Paumgartner, G., Gerbes, A.L., 1999. Prevention of Kupffer cell-induced oxidant injury in rat liver by atrial natriuretic peptide. Am. J. Physiol. 276, G1137–G1144.
Mittler, R., 2002. Oxidative stress, antioxidants and stress tolerance. Trends Plant Sci. 7, 405–410.
Dorval, J., Hontela, A., 2003. Role of glutathione redox cycle and catalase in defense against oxidative stress induced by endosulfan in adrenocortical cells of rainbow trout (*Oncorhynchus mykiss*). Toxicol. Appl. Pharmacol. 192, 191–200.
Gouaze, V., Andrieu-Abadie, N., Cuvillier, O., Malagarie-Cazenave, S., Frisach, M.F., Mirault, M.E., Levade, T., 2002. Glutathione peroxidase-1 protects from CD95-induced apoptosis. J. Biol. Chem. 277, 42867–42874.
Sanyal, A., 2001. Nonalcoholic steatohepatitis. Indian J. Gastroenterol. 20 (Suppl. 1), C64–C70.
Anstee, Q.M., Goldin, R.D., 2006. Mouse models in non-alcoholic fatty liver disease and steatohepatitis research. Int. J. Exp. Pathol. 87, 1–16.
Yamaguchi, K., Yang, L., McCall, S., Huang, J., Yu, X.X., Pandey, S.K., Bhanot, S., Monia, B.P., Li, Y.X., Diehl, A.M., 2007. Inhibiting triglyceride synthesis improves hepatic steatosis but exacerbates liver damage and fibrosis in obese mice with nonalcoholic steatohepatitis. Hepatology 45, 1366–1374.
Herrera, B., Alvarez, A.M., Sanchez, A., Fernandez, M., Roncero, C., Benito, M., Fabregat, I., 2001. Reactive oxygen species (ROS) mediates the mitochondrial-dependent apoptosis induced by transforming growth factor (beta) in fetal hepatocytes. FASEB J. 15, 741–751.
Simon, H.U., Haj-Yehia, A., Levi-Schaffer, F., 2000. Role of reactive oxygen species (ROS) in apoptosis induction. Apoptosis 5, 415–418.
Wheeler, M.D., 2003. Endotoxin and Kupffer cell activation in alcoholic liver disease. Alcohol Res. Health 27, 300–306.
Su, G.L., 2002. Lipopolysaccharides in liver injury: molecular mechanisms of Kupffer cell activation. Am. J. Physiol. Gastrointest. Liver Physiol. 283, G256–G265.
Kitamura, K., Nakamoto, Y., Akiyama, M., Fujii, C., Kondo, T., Kobayashi, K., Kaneko, S., Mukaida, N., 2002. Pathogenic roles of tumor necrosis factor receptor p55-mediated signals in dimethylnitrosamine-induced murine liver fibrosis. Lab. Invest. 82, 571–583.
Tomita, K., Tamiya, G., Ando, S., Ohsumi, K., Chiyo, T., Mizutani, A., Kitamura, N., Toda, K., Kaneko, T., Horie, Y., Han, J.Y., Kato, S., Shimoda, M., Oike, Y., Tomizawa, M., Makino, S., Ohkura, T., Saito, H., Kumagai, N., Nagata, H., Ishii, H., Hibi, T., 2006. Tumour necrosis factor alpha signalling through activation of Kupffer cells plays an essential role in liver fibrosis of non-alcoholic steatohepatitis in mice. Gut 55, 415–424.